

Opposing Rigidity-Protein Gradients Reverse Fibroblast Durotaxis

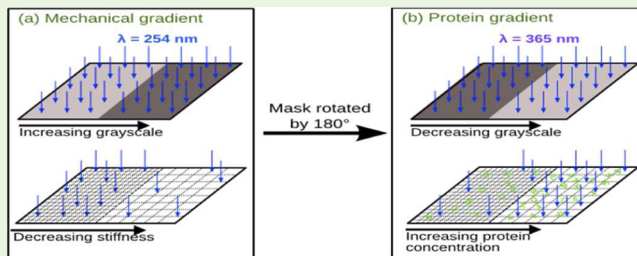
Gaurav Jain,^{†,‡} Andrew J. Ford,^{†,§} and Padmavathy Rajagopalan^{*,†,‡,§,⊥}

[†]School of Biomedical Engineering and Sciences, [§]Department of Chemical Engineering, and [⊥]ICTAS Center for Systems Biology of Engineered Tissues, Virginia Tech, Blacksburg, Virginia 24061, United States

Supporting Information

ABSTRACT: The migration of cells is a complex and dynamic process that is governed by several stimuli acting simultaneously. *In vivo*, cells receive and process a wide range of cues that guide their motion and migratory characteristics such as speed and directionality. The design of biomaterials that can recapitulate the combinatorial signaling environment can aid in understanding how migrating cells respond to more than one stimulus and when one cue dominates over the other. We have designed hydrogel substrates that exhibit opposing rigidity-and collagen gradients. Within the boundaries of the interfacial region, the values for substrate modulus decreased in one direction with a concomitant increase in the concentration of surface-bound collagen. The well-known durotactic migration of fibroblasts was first validated on substrates that only exhibit a gradient in modulus while keeping the concentration of surface-bound collagen constant. Upon increasing the collagen concentration on the low-modulus regions by 4- or 7-fold compared to the high-modulus side of the interface, cells exhibited directed migration toward the soft regions of the substrate. This effect was more pronounced when the surface-bound collagen concentration was 7-fold greater. Cell displacements, areas, cytoskeleton and focal adhesions were investigated on the opposing rigidity-immobilized collagen gradients. These features were affected by the elastic modulus of the substrate as well as the change in protein concentration. In the future, incorporating multiple gradients within a single substrate will lead to a deeper and more comprehensive understanding of cells navigate through the complex *in vivo* microenvironment.

KEYWORDS: cell migration, durotaxis, haptotaxis, directed migration



INTRODUCTION

The locomotion of cells is integral to several physiological processes such as developmental biology,^{1–3} wound healing,⁴ inflammation,⁵ disease progression,^{6–8} and the maintenance of tissue homeostasis.⁹ *In vivo*, cells frequently exhibit directional migration toward a specific location because of signals received from their extra-cellular microenvironment and from cell–cell interactions.^{10–15} Cells respond to a wide range of guiding cues. These external stimuli can be mechanical,^{16,17} electrical,¹⁸ optical,¹⁹ extent of hydration,²⁰ or chemical in nature. Moreover, migration is often controlled by such stimuli in order to guide cells toward specific locations within healthy and injured tissues.^{21,22} When there is more than one guiding cue for cell migration, it remains unclear to what extent each stimulus controls the directionality of motion. This is of particular significance at junctions of tissues where gradients in protein concentrations and substrate stiffness may coexist.²³ This question assumes particular significance in multicellular organisms, which contain assemblies of interconnected tissues that involve interfacial regions with significantly different chemical and mechanical properties on each side. Examples include the osteochondral interface,^{24,25} the muscle-tendon junction,^{26,27} and the breast-bone region.^{28–30} Even within a single tissue, the environments through which cells migrate can be anisotropic because of variations in protein concentrations

and composition, rigidity of the underlying substrate, and changes in topography or porosity.

The effects of varying substrate rigidity or protein concentration on cell migration have been widely investigated using *in vitro* systems.^{16,17,31–35} It has been shown that cells can sense changes in the substrate rigidity or the concentration of chemicals in their microenvironment and respond by altering their direction of migration.^{16,17,33,36–41} Chemotaxis (migration due to a soluble chemical gradient), haptotaxis (motion due to an immobilized chemical gradient), and durotaxis (locomotion as a function of substrate rigidity) have been widely observed and studied for many types of cells.^{28,42,43} Despite the need to understand locomotion occurring in the presence of complex and opposing signals, in a majority of these studies, the migration of cells has been investigated upon varying only one guiding cue.^{23,28} A fundamental question in cell migration that remains unanswered is how different and potentially conflicting signals are processed by a cell in order for it to make a decision on the directionality and extent of motion.

Investigations into cell migration have focused primarily on either the effects of varying substrate rigidity or ligand concentration.^{16,17,33,39–41} To the best of our knowledge,

Received: October 27, 2014

Accepted: July 10, 2015

Published: July 10, 2015

there are very few reports on the combinatorial effect of physical and chemical cues on cell migration. Sundararaghavan and co-workers designed electrospun scaffolds with gradients in elastic modulus and RGD (arginine-glycine-aspartic acid) density.⁴⁴ In these scaffolds increasing the modulus and ligand density in the same direction led to higher cell areas and infiltration. Kim et al. have reported that the spreading of human mesenchymal stem cells (hMSCs) was unaffected by substrate rigidity in the presence of high RGD densities.⁴⁵ We have previously reported that fibroblasts move toward a softer substrate if it also contained a high protein concentration.⁴⁶ In this study, migration was investigated at a sharp interface where regions with distinctly different elastic moduli were obtained on either side. The interface was designed by a two-drop method and resulted in a very narrow interface ranging from 12 to 35 μm . Collagen was presented in the form of protein-coated beads. The concentration of collagen-coated beads was higher on the low-modulus side of the interface. The substrates exhibited a very sharp transition from low- to high-modulus regions and did not exhibit gradients in mechanical and chemical properties.

In this study, our goal was to determine if cells were presented with a choice to move toward a soft/high protein or a stiff/low protein region within a substrate, which direction would they choose to move? We sought to discover whether a phenomenon as widely studied as durotaxis could potentially be reversed if cells were presented with another attractive migratory stimulus. Specifically, we investigated how strong a chemical cue would have to be for fibroblasts to move away from a rigid region on a biomaterial. To this end, we designed and assembled hydrogel substrates that exhibit opposing gradients in substrate rigidity and protein concentrations. We report a hydrogel assembly method that results in interface widths of about 150 μm that are much closer to those found in vivo such as in skin. The properties gradually change from end of the interface to the other. We have introduced two very different protein gradients to determine how shallow or steep the protein gradients need to be in order for cells to reverse durotaxis. These studies are very relevant to wound healing scenarios where protein concentrations guide directed migration. We have assembled two different protein gradients where the increase in collagen concentration is either 4- or 7-fold from the high- to low-modulus regions. We monitored fibroblast migration within the boundaries of the interfacial region to determine which cue would guide directionality.

EXPERIMENTAL SECTION

Materials and Methods. *Materials.* Fluorescein isothiocyanate (FITC) labeled collagen ($M_w = 1 \times 10^6$ Da), 4-(2-hydroxyethyl)-1-piperazineethanesulfonic acid (HEPES) buffer, Irgacure 2959 (1-[4-(2-hydroxyethoxy)-phenyl]-2-hydroxy-2-methyl-1-propane-1-one) and 3-triethoxysilylpropylamine (3-APTES) were purchased from Sigma-Aldrich, St Louis, MO. Glutaraldehyde (25% v/v) was purchased from Electron microscopy Sciences, Hatfield, PA. Phosphate buffered saline (PBS), rhodamine-conjugated polystyrene (PS) beads (0.5 μm in diameter), penicillin-streptomycin and Dulbecco's modified Eagle medium were purchased from Invitrogen Life Technologies, Carlsbad, CA. Acrylamide (10% v/v), bis-acrylamide (0.72 v/v), and ammonium persulfate (APS) were purchased from Bio-Rad, Hercules, CA. All other chemicals and supplies were purchased from Thermo Fisher Scientific Waltham, MA unless otherwise specified.

Design of Polyacrylamide (PAAM) Substrates with Opposing Rigidity and Protein Gradients. Glass coverslips were activated using previously published procedures.^{46,47} All PAAM hydrogels in this

study were polymerized using monomer solutions that contained acrylamide (10% v/v), bis-acrylamide (0.72% v/v), and APS.

Creating Gradients in Substrate Rigidity. High-resolution photo-masks (2 $\mu\text{m}/\text{pixel}$) with difference gray scale values were custom-designed on chrome substrates (Benchmark Technologies, Lynnfield, MA). Gray scale masks with four different transmittance values were designed to control the intensity of incident UV radiation (Figure 1).

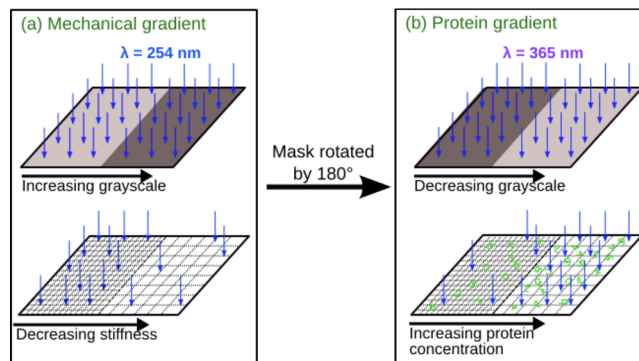


Figure 1. Design and assembly of hydrogels that exhibit opposing rigidity and protein gradients. UV-mediated polymerization and chemical conjugation at two separate wavelengths were used to cross-link and conjugate collagen.

The mask was placed in a custom-designed holder in order to precisely rotate it during hydrogel assembly. Below, the percentage value in a mask represents the amount of light transmitted through the mask. A higher percentage value corresponds to a greater light transmittance, which results in higher degrees of cross-linking. The differential absorption of UV light resulted in changes in the extent of cross-linking and the generation of an interfacial region with two distinct elastic moduli.^{3,48} Rigidity gradients were obtained using two combinations of gray scale values: 70%/40% (denoted as Mask 1) and 80%/30% (denoted as Mask 2).

Polymerization was initiated by Irgacure 2959 (1.2% w/v)⁴⁹ and UV radiation (UVP, Upland CA). The UV wavelength and intensity were 254 nm and 15 mW/cm², respectively. Rhodamine-conjugated PS beads (~0.5 μm in diameter) were added to all monomer solutions to enable the identification of the rigidity gradient. In the PAAM hydrogel, low and high-cross-linking resulted in "soft" and "stiff" regions, respectively. The interfacial region was defined as the area between the lowest and highest values for substrate rigidity.

Creating Gradients in Immobilized Collagen. Gradients in immobilized collagen were generated on hydrogels exhibiting uniform elastic modulus as well as on gels exhibiting a gradient in elastic modulus. The immobilization of collagen was conducted using the same chemical reaction on both types of hydrogels. For hydrogels exhibiting gradients in rigidity, the concentration of surface-immobilized collagen was increased in the opposite direction of the rigidity gradient. FITC-labeled Type 1 collagen was conjugated to PAAM gels using N-hydroxyl succinimide (NHS) and a hetero bifunctional cross-linker (sulfo-succinimidyl-diazirine (SDA)). Reaction time with SDA and the concentration of collagen were varied to optimize the efficiency and yield of FITC-collagen. The collagen gradient was superimposed on the rigidity gradient by rotating the gray scale mask by 180° and exposing to UV light (365 nm; Spectroline, Westbury, NY) at an intensity of 27 mW/cm² (Figure 1). The protein gradients were generated by UV exposure for 10 min and 30 μL of collagen deposited on the "soft" or "stiff" regions. The input collagen concentration varied from 15 to 50 $\mu\text{g}/\text{mL}$. PAAM gels were rinsed in 50 mM HEPES (pH 7) for up to 48 h and stored at 4 °C.

Atomic Force Microscopy (AFM). The surface topography of hydrated PAAM gels was obtained using a Veeco Bioscope II AFM (Veeco, Santa Barbara CA). All measurements were conducted in contact mode using pyramidal SiN cantilever tips (Bruker AFM Probes, Camarillo, CA) with a spring constant of 0.12 N m⁻¹. The

hydrogel area scanned was $10 \times 10 \mu\text{m}$. AFM measurements were conducted at the center of the interfacial region and at $\pm 100 \mu\text{m}$ of this point. AFM images were collected at a minimum of 3 separate locations in each of these regions. The root-mean-square (RMS) surface roughness was calculated from these images using Veeco diNanoscope Software 7.0.

Young's modulus (YM) measurements of hydrogels were obtained on hydrated samples using a Veeco MultiMode AFM (Veeco, Santa Barbara CA). All measurements were conducted in contact mode using pyramidal SiN cantilever tips (Bruker AFM Probes, Camarillo, CA) with a spring constant of 0.12 N m^{-1} . The force–distance curves were obtained at 1 Hz using the blunted tips with a half open angle of 18° . The elastic modulus was obtained by fitting the raw data to a modified Hertz cone model using eqs 1 and 2.

$$F = k(d - d_0) \quad (1)$$

$$F = \frac{2\tan \alpha}{\pi} \left[\frac{E}{1 - \nu^2} \right] \delta^2 \quad (2)$$

where F = applied force, $\alpha = 18^\circ$, E = YM, k = spring constant of the cantilever, ν = Poisson's ratio (constant = 0.4),^{50,51} d = deflection of the cantilever, and δ = indentation.

Initial Identification of the Interfacial Region Using Fluorescence Microscopy. the YM of gradient gels was determined by initial identification of the interfacial region through fluorescence microscopy. Fluorescent imaging was conducted on a Nikon TE 2000 inverted microscope to determine the intensity of rhodamine beads. Fluorescent intensity was calculated using Nikon Elements software. This value was used to determine fluorescent intensities at the high and low cross-linked regions. In hydrogels assembled using either Masks 1 or 2, a 15% difference in intensity was observed between high- and low- cross-linked regions. These values were only used to identify the initial boundaries of the interfacial region.

Refinement of the Interfacial Region Using YM Measurements. The precise locations of the boundaries were determined by conducting multiple AFM measurements. The center of the interfacial region obtained by fluorescence microscopy was designated as the (0,0) position. Measurements were conducted at ± 12.5 , 25 , 37.5 , 50 , 100 , 150 , and $200 \mu\text{m}$ of the center coordinates at three different positions along the same interfacial region. These measurements were conducted on three separate gels per gradient condition. The boundaries of the interfacial region were established using the following procedure. In a hydrogel with a rigidity gradient introduced by Mask 1, YM values obtained at each position within the gradient were compared to those obtained from corresponding homogeneous gels. YM values were compared (using a *t*-test with α set to 0.05) to those obtained for gels polymerized using only a 70% or a 40% mask. The last position at which the YM value was found to be statistically significant ($p < 0.05$) when compared to a gel polymerized with an 70% or 40% mask was identified as the boundary on the stiffer and softer side, respectively. Similar measurements were conducted for gradients generated with Mask 2. The migratory behavior of cells was investigated only within this rigidity gradient.

Concentration of Surface-Immobilized Collagen. The surface density of collagen was measured by a fibronectin (FN) binding assay.⁵² Briefly, FITC-collagen (Type 1) ranging from 15 – $50 \mu\text{g/mL}$ in concentration was covalently conjugated either to PAAM gels or dried on tissue culture polystyrene (TCPS, control) wells. FN (BD Biosciences) was biotinylated using a commercially available kit (Thermo Fisher Scientific) as per the manufacturer's protocol. The substrates were incubated with biotinylated fibronectin and horseradish peroxidase-streptavidin. Thereafter, tetramethylbenzidine (TMB) was added and the absorbance at 450 nm was measured on a microplate reader (Molecular Devices, Sunnyvale, CA). The input concentration of collagen on the "soft" substrates was either $30 \mu\text{g/mL}$ or $50 \mu\text{g/mL}$. In order to measure the surface density of collagen, standards were prepared by adsorbing different input concentrations of collagen onto TCPS at 37°C for 16 h in a humidified environment and then at 40°C for 24 h at room temperature. Assuming 100% binding efficiency on TCPS,^{52,53} a calibration curve was obtained which was

used to calculate the binding efficiency of collagen conjugated to low and high modulus gels (Figure S1). The intensity obtained from proteins adsorbed to the glass coverslips was measured independently and subtracted from the final value. Surface values were calculated by assuming a cylindrical gel with a height of $45 \mu\text{m}$ (height of a typical PAAM gel in this study) and a diameter of 15 mm (diameter of coverslips on which gels were cast).

Cell Culture. Murine Balb/c 3T3 cells (Balb/3T3 clone A31, American Type Culture Collection, Manassas, VA) were maintained between passage numbers 3 to 15 at 37°C under a humidified atmosphere at 5% CO_2 . Cells were maintained in DMEM supplemented with 10% v/v bovine calf serum (Hyclone, Logan, UT) and 2% v/v penicillin-streptomycin.

Time Lapse Microscopy. PAAM gels were sterilized by exposure to germicidal UV for 1 h. Fibroblasts (at a density of $80\,000 \text{ cells/cm}^2$) were cultured on the hydrogels for 6–8 h prior to conducting microscopy. The gels were placed in a closed observation chamber (Biotech, Butler, PA) maintained at 37°C . This chamber was perfused with CO_2 -enriched culture medium at a rate of 1 mL/min .⁵⁴ Phase contrast and fluorescent images were obtained on an inverted TE-2000U Nikon microscope every 30 min up to 6 h. Cells that underwent death, mitosis, exited the frame, or collided with adjacent cells during the observation period were not taken into consideration for further analysis. To calculate cell speed and displacement, the "x" and "y" coordinates of the cell centroids were measured at each time point. The mean-squared displacement ($\langle d^2 \rangle$) was calculated for a cell tracked for a total time $t_{\max} = N\Delta t$ with a series of real time coordinates ($x(n\Delta t)$, $y(n\Delta t)$), eq 3.³⁸ Here, N is the total number of time-points at which coordinates were obtained, whereas n and i are intermediate time-points.

$$\begin{aligned} \langle d^2 \rangle, t = n\Delta t \\ = \frac{1}{(N - n + 1)} \sum_{i=0}^{i=N-n} [(x((n+1)\Delta t) - x(i\Delta t))^2 \\ + (y((n+1)\Delta t) - y(i\Delta t))^2] \end{aligned} \quad (3)$$

Only those cells that exhibited a minimum mean square displacement of $30 \mu\text{m}$ over the 6 h observation period were further investigated for directionality of locomotion. This cutoff value was very close to the width of fibroblasts on the hydrogel substrates.

Immunofluorescence Staining for Actin and Vinculin. PAAM hydrogels were polymerized with $0.5 \mu\text{m}$ fluorescent blue beads (Polysciences Inc., Warrington PA). Fibroblasts were fixed using a 0.75% glutaraldehyde in 1X PBS (v/v, Electron Microscopy Sciences, Hatfield PA) solution. A 0.1% Triton X-100 (Sigma-Aldrich) solution was added to enhance membrane permeability. Samples were incubated at 37°C for 2 h in a 0.1% AlexaFluor 350 phalloidin (Invitrogen Life Technologies) solution and a monoclonal antibody to vinculin (Abcam; 1:100 dilution) followed by a FITC-conjugated secondary antibody (Abcam; 1:100 dilution). Images were obtained on a Zeiss LSM 510 Laser scanning confocal microscope placed on an inverted Axio Observer Z1 base.

Profilometry. A Veeco Dektak 150 (Bruker, Billerica, Massachusetts) profiler was used to determine the hydrated thickness of PAAM substrates. The location of the interface was first identified and marked. Thereafter, measurements were taken every $50 \mu\text{m}$ from the interface.

Statistical Analysis. Statistical significance and *p*-values between sample groups (e.g., evaluating trends in cell areas and displacement) were determined by *t* test analysis with alpha set to 0.05. All data are reported as mean \pm standard deviation. Sample sizes are denoted by n and were obtained from at least 3 separate experiments per gel condition.

The binomial test was performed to assess the statistical significance of the cell count trends in cell migration. For rigidity gradients, the null hypothesis was that cells would not show a preference to migrate toward either side of the interface. Hence, according to the null hypothesis, the probability that a cell would move toward the high modulus side of the interface was 0.5. Suppose that out of a total of l

cells, we observed k cells moving toward the high modulus side, where k was larger than $l/2$. Then the alternative hypothesis was that cells showed a preference to move toward the high modulus side. Under the null hypothesis, the probability that we would observe k or more out of l cells moving toward this side is provided in eq 4. This quantity is the p -value of the one-sided binomial test. The one-sided binomial test was appropriate here because of the way in which the alternative hypothesis is posed: that the cells moved toward the high modulus side. Alpha was maintained at a value of 0.05. Cells exhibiting random walk motion within 30 μm of the high-modulus edge of the interfacial region were not included in k .

$$\text{bin}(l, k, 1/2) = \sum_{i=k}^l \binom{l}{i} \left(\frac{1}{2}\right)^i \left(\frac{1}{2}\right)^{l-i} = \sum_{i=k}^l \binom{l}{i} \left(\frac{1}{2}\right)^l \quad (4)$$

On the basis of the results described later for rigidity gradients, the null hypothesis for dual gradients was that cells would show a preference to migrate toward the high-modulus/low-protein side of the interface. Hence, according to the null hypothesis, the probability that a cell would move toward the low-modulus/high-protein side of the interface was p , where this probability was calculated from the cell counts for rigidity gradients. Suppose that out of a total of l cells, we observed k cells moving toward the low-modulus/high-protein side, with k being at least $l/2$. The alternative hypothesis was that the cells showed a preference for the low modulus/high protein side. Then, under the null hypothesis, the probability that we would observe k or more out of l cells moving toward this side is provided in eq 5. This quantity is the p -value of the one-sided binomial test. Alpha was maintained at a value of 0.05. Cells exhibiting random walk motion within 30 μm of the high-modulus edge of the interfacial region were not included in k .

$$\text{bin}(l, k, p) = \sum_{i=k}^l \binom{l}{i} p^i (1-p)^{l-i} \quad (5)$$

RESULTS

Design of Rigidity Gradients. PAAM hydrogels were first polymerized using a photomask with a single gray scale value of 80, 70, 40, or 30%. The elasticity of these hydrogels guided the design of rigidity gradients (RGs). The Young's modulus of these hydrogels was 126.7 ± 1.9 kPa (80%, $n = 3$), 80.7 ± 6.2 kPa (70%, $n = 3$), 48.2 ± 2.7 kPa (40%, $n = 3$) and 46.7 ± 1.2 kPa (30%, $n = 3$). On the basis of these values, two rigidity gradients RG1 and RG2 were obtained using Mask 1 and 2, respectively. The fold change in elastic modulus between the soft and stiff regions was either ~ 1.7 (RG1) or 2.7 (RG2). The values of YM ratios were in close agreement to the differences in UV transmittance within each mask. In Mask 1 (70%/40%) and Mask 2 (80%/30%), the fold differences in the gray scale values were 1.75 and 2.66, respectively. On RG1, the YM values at approximately 33% and 66% of the interfacial width were 50.7 ± 9.88 kPa and 66.0 ± 6.49 kPa, respectively. On RG2, the YM values at approximately 33% and 66% of the interfacial width were 67.4 ± 7.03 and 75.8 ± 7.94 kPa, respectively. The values of elastic modulus at these regions were statistically different from each other and from the low and high values of the interfacial modulus. The gradually increasing values of YM demonstrate that RGs were obtained using the UV photo masks. The widths of the interfacial regions were determined upon immobilizing collagen (Type 1; 15 $\mu\text{g}/\text{mL}$) prior to conducting measurements. The interfacial widths were 95.8 ± 14.4 μm and 158.3 ± 23.6 μm for hydrogels assembled with Masks 1 and 2, respectively (Table 1). The interfacial width generated by Mask 2 was significantly higher due to the greater differential in gray scale values and unavoidable refraction of

Table 1. Width of Rigidity and Dual Gradients Using AFM Measurements

rigidity gradient (RG)		dual gradient (DG)	
substrate	width (μm)	substrate	width (μm)
RG1	95.8 ± 14.4 ($n = 3$)		none
RG2	158.3 ± 23.6 ($n = 3$)	DG1	158 ± 11.8 ($n = 3$)
		DG2	150 ± 20.4 ($n = 3$)

UV light. Together, these factors resulted in cross-linking across a larger cross-section of the gel.

Fibroblast Migration on Rigidity Gradients. Durotaxis was monitored on two different rigidity gradients. Approximately 65% (RG1) and 74% (RG2) of cells either migrated toward the stiffer regions of the hydrogel or exhibited random walk motion at the rigid edge of the gradient (Table 2, Figure 2,

Table 2. Direction of Fibroblast Migration on Rigidity Gradients

Direction of motion	RG1 $n = 23$	RG2 $n = 34$
soft to stiff	13	20
stiff to soft	8	9
exhibiting random walk motion near the high-modulus edge of the interfacial region	2	5
<i>p</i> -value of binomial test	0.2	0.03

Videos S3 and S4). The average values for total displacement were 45 ± 17.8 μm (RG1) and 71.5 ± 25.3 μm (RG2). However, when the displacements over each 2 h period were calculated, significant differences were observed between the two gradients (Figure 3A, E). On RG1, the average displacement was 32.9 ± 11.0 , 17.1 ± 7.2 , and 9.6 ± 5.9 μm from 0–2, 2–4, and 4–6 h, respectively. In contrast, on RG2, fibroblasts exhibited average displacements of 25.6 ± 10.8 μm , 21.3 ± 14.6 μm , and 25.1 ± 14.9 μm in the same time periods. These trends indicate that fibroblasts remained motile on RG2 throughout the observation period in contrast to the large decrease in speed observed on RG1 in the second half. Moreover, changes in spread cell areas (Figure 3B, F) were observed between the two gradients. Approximately 43% (RG1), and 35% (RG2) of cells exhibited increased cell areas ($\text{Area}_{6h}/\text{Area}_{0h} > 1$) (Figure 3B, F). An increase in cell area is indicative of changes in adhesivity as the cells migrate along the gradient substrates. The significantly higher cell areas on RG1 (Table S1) suggest that the cell adhesion to the underlying substrate is greater in comparison to RG2 ($p_{t=0h} = 0.005$, $p_{t=6h} = 0.0001$). The individual tracks of the cells analyzed show there is a clear preference exhibited by fibroblasts for the high-modulus regions of the interface (Figures 3C and 3G). This was further illustrated when the average trajectory of all cells was calculated (Figure 3D, H). The extended migratory behavior of fibroblasts on RG2 compared to RG1 can be attributed to the differences in the widths of the two interfacial regions. Fibroblasts moving on RG2 have to migrate a wider distance in order to reach the rigid edge of the interface and would therefore remain motile for longer time periods. Upon applying the one-sided binomial test to the data show in Table 2, the *p*-values for RG1 and RG2 were calculated to be 0.2 and 0.03, respectively. Therefore, the results obtained on RG1 were not significant. In contrast, migration to the high modulus region was statistically significant for RG2 at the 0.05 level.

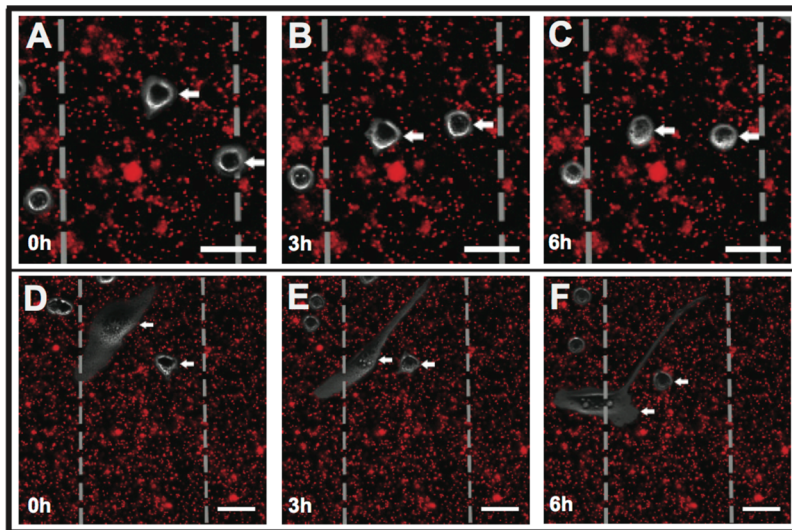


Figure 2. Merged phase-contrast and fluorescence time-lapse images of fibroblasts migrating on (A–C) RG1 and (D–F) RG2. Durotactic motion is observed on both rigidity gradients over a 6 h period. Scale bars = 50 μ m.

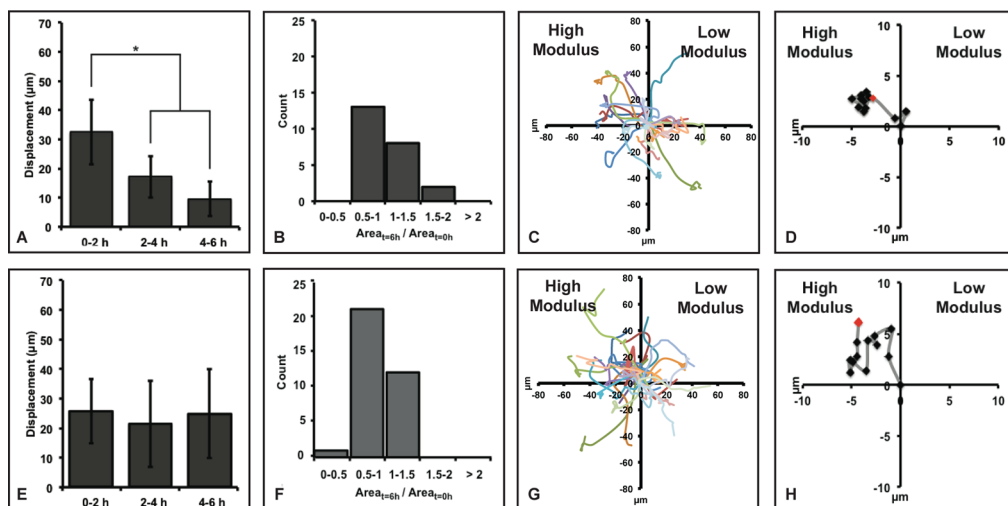


Figure 3. Average displacements exhibited by fibroblasts over 2 h increments on (A) RG1 and (E) RG2. Histograms of the area fold change exhibited by fibroblasts over 6 h on (B) RG1 and (F) RG2. Individual tracks of all cells analyzed on the rigidity gradients (C) RG1 and (G) RG2. The average trajectory of all cells analyzed on the rigidity gradients (D) RG1 and (H) RG2. The diagrams show positions at each time-point relative to the cell's initial position ($t = 0$). An asterisk (*) indicates a statistically significant difference ($p < 0.05$). $n = 23$ cells from 3 separate experiments (RG1) and $n = 34$ cells from 3 separate experiments (RG2).

Design of Dual Gradients. RG2 was selected to superimpose a collagen gradient in the opposite direction. This gradient was chosen due to statistically significant durotaxis exhibited by fibroblasts. This substrate exhibited statistically significant changes in YM across the interfacial region. Moreover, the greater width of this rigidity gradient would pose an additional challenge for cells because they would have to migrate a greater distance away from the stiff side of the RG to reach locations with high collagen concentration. Two different chemical gradients were superimposed in the opposite direction to the rigidity gradient as follows. On the stiff side of RG2 (which exhibited a YM of 126.7 ± 1.9 kPa), the input concentration of protein was $15 \mu\text{g}/\text{mL}$. On the soft side of RG2 (YM of 46.7 ± 1.2 kPa), the input concentration of protein was either 30 or $50 \mu\text{g}/\text{mL}$. Upon exposure to UV light, the immobilized protein concentration varied between the low and high YM boundaries of the rigidity gradient. On the stiff

side, the surface concentration of collagen was 3.5 ± 1.2 molecules/ μm^2 . On the soft side, the surface concentration of collagen was 12.7 ± 6.2 or 23.9 ± 5.7 molecules/ μm^2 , corresponding to the input concentrations of 30 or $50 \mu\text{g}/\text{mL}$, respectively. Thus, the collagen concentrations increased either 4- or 7-fold from the rigid to the soft regions of the substrate. Henceforth, these dual gradients will be denoted as Dual gradient 1 (DG1, 4-fold increase) and Dual gradient 2 (DG2, 7-fold increase). The width of RG2 did not undergo a significant change upon superimposing the collagen gradient (Table 1). Fluorescent images of a typical dual gradient are presented in Figure 4.

The RMS surface roughness of the DG1 and DG2 hydrogels was determined through atomic force microscopy. The surface roughness of these hydrogels did not change across the interfacial region for either the DG1 or the DG2 hydrogels (Figure 5). RMS surface roughness values of 5.34 ± 0.51 , 4.94

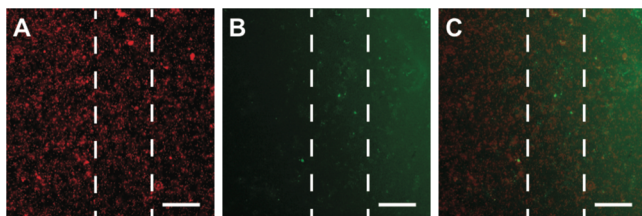


Figure 4. Fluorescent images of: (A) rhodamine-conjugated polystyrene beads imbedded within the PAAM hydrogel; (B) FITC-conjugated type 1 collagen bound to the hydrogel surface; (C) merged fluorescence images of the hydrogel substrate. The vertical dotted lines correspond to the boundaries of the interfacial region. Scale bar = 100 μm .

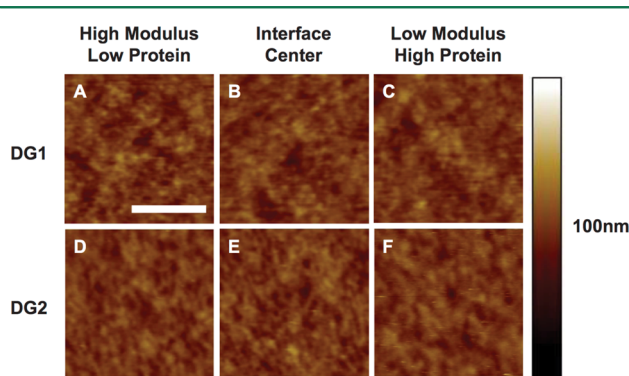


Figure 5. AFM images of the hydrogel surface at (A, D) the stiff/low protein side of the interface, (B, E) the interface center, and (C, F) at the soft/high protein side of interface for the DG1 and DG2 gels. Scale bar = 5 μm .

± 0.50 , and 4.67 ± 0.17 nm were obtained at the high modulus/low protein side of the interface, the center, and at the low modulus/high protein side of interface for the DG1 gels. At the exact locations, these values were 5.09 ± 0.38 , 4.71 ± 0.30 , and 4.42 ± 0.13 nm for the DG2 gels. These values were found to be statistically insignificant.

Design of Chemical Gradients. Gradients in immobilized collagen concentration were generated on hydrogels exhibiting an intermediate, homogeneous stiffness. The average YM within $\pm 25 \mu\text{m}$ of the center of the RG2 gradients was 66.3 ± 8.83 kPa. We chose this value of Young's modulus since it was similar to values obtained in the middle of the interfacial region of RG2. This hydrogel was UV polymerized using the 70% gray scale mask. On one side of these hydrogels, the input concentration of protein was $15 \mu\text{g/mL}$ corresponding to a surface concentration of 3.5 ± 1.2 molecules/ μm^2 . On the alternate side, input concentration was $50 \mu\text{g/mL}$ corresponding to a surface concentration of 23.9 ± 5.7 molecules/ μm^2 . These gels, which exhibit a 7-fold increase in collagen concentration across the gradient, will be denoted as chemical gradient 1 (CG1).

Fibroblast Migration on Chemical Gradients. On CG1 hydrogels, approximately 74% of cells exhibited motion toward the high protein side of the interface or performed random walks in this region (Table 3). Of the remaining 26%, half of these cells migrated primarily in the vertical direction along the interfacial region. Fibroblasts exhibited average displacements of $79.0 \pm 33.9 \mu\text{m}$ over the 6 h period, comparable to the displacements of cells on RG2 gels. Average displacements of fibroblasts over each 2 h period were found to be $25.9 \pm 16.7 \mu\text{m}$, $25.5 \pm 13.9 \mu\text{m}$, and $27.6 \pm 21.8 \mu\text{m}$ from 0–2, 2–4, and

Table 3. Direction of Fibroblast Migration on Chemical Gradients

Direction of motion	CG1 n = 38
low to high protein	27
high to low protein	10
exhibiting random walk motion near the high-protein edge of the interfacial region	1
p-value of binomial test	0.0038

4–6 h, respectively (Figure 6A). Approximately 55% of fibroblasts exhibited an increase in projected cell area (Figure 6B). As illustrated by the cell angularity, the individual cell tracks and average trajectory of all cells, there is a clear preference exhibited by fibroblasts for the high-protein regions of the interface (Figure 6C–E). The directionality toward the high protein region was statistically significant with a p-value of 0.0038.

Fibroblast Migration on Opposing Rigidity/Protein Gradients.

Fibroblasts migrating across DG1 or DG2 were monitored to determine their preference for directed motion toward the 46 kPa (soft) edge of the interfacial region (Figure 7, Table 4, Videos S3 and S4). On DG1, approximately 62% of cells either migrated toward the soft edge or exhibited random walks on the soft/high protein edge of the gradient. When a 7-fold increase in collagen was introduced (DG2) a dramatic increase in the preferred direction of migration was noted with 73% of cells clearly exhibiting motion toward the 46 kPa region or performing random walks in this region as shown by the individual cell tracks (Figure 8A, C). Approximately, 38% and 27% of fibroblasts migrated toward the high modulus region on the DG1 and DG2 substrates, respectively. Upon tracking the average trajectories of all cells (Figures 8B, D), both dual gradients elicited cells migrating toward the high collagen/low-modulus regions. However, fibroblasts clearly infiltrated DG2 to a greater extent. Please refer to Figure 2C, D for trajectories of all cells.

The binomial test was repeated for the data in Table 4. Because both dual gradients were assembled with the stiffness gradient from RG2, according to the null hypothesis, the probability that a cell would move to the high-collagen/low-modulus side was 0.31 (9/29; see Table 2). The p-values of the one-sided binomial test with this probability were for 0.004 for DG1 and 3×10^{-5} for DG2. Therefore, fibroblasts on both dual gradients exhibited a reversal of durotaxis. Comparing the cell trajectories in Figure 8B, D, infiltration of fibroblasts into the low-modulus/high-collagen regions is greater only when the collagen concentration is 7-fold higher (Figure 8D). When the collagen concentration is 4-fold higher (Figure 8B), the cells enter the low modulus region but do not infiltrate it to a great extent.

The locomotion of cells across the two dual gradients revealed additional interesting contrasts. Projected cell areas and fold changes in cell areas on DG2 were statistically higher ($p < 0.05$) in comparison to cells moving on the corresponding rigidity gradient (RG2) (Table S1, Figure 8E). The average displacement from 0–3 h was also lower for cells on DG2 when compared to RG2 or DG1 (Figure 8F). Because cells do not move in a linear manner, the angle (θ) made by the line connecting the final and initial coordinates for each cell with the x-axis was calculated. If this angle ranged between $\pm 45^\circ$ the cell would have moved primarily in the positive "x" direction (toward the soft/high protein side of the dual gradient).

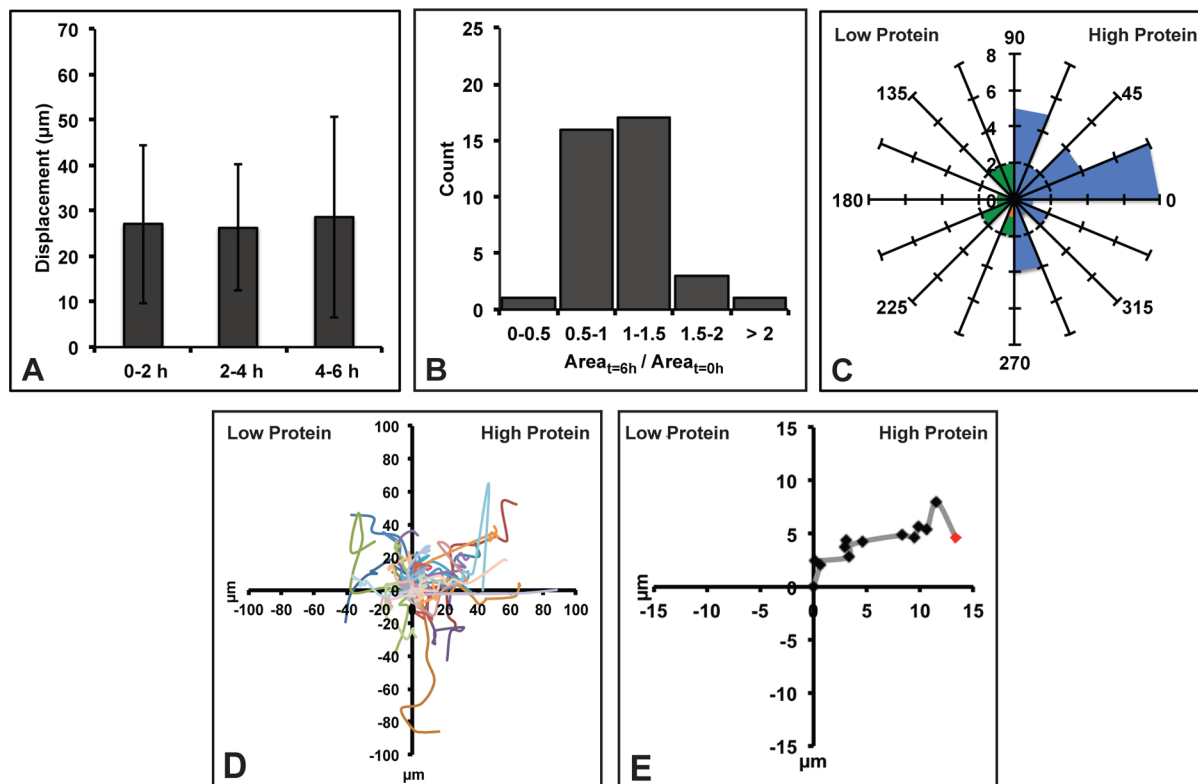


Figure 6. (A) Average displacements exhibited by fibroblasts over 2 h increments on CG1. (B) Histograms of the area fold change exhibited by fibroblasts over 6 h on CG1. (C) Angularity histogram for fibroblasts on the chemical gradients. (D) Individual tracks of all cells analyzed on the chemical gradient CG1. (E) The average trajectory of cells analyzed on the chemical gradients. The diagram show positions at each time-point relative to the cell's initial position ($t = 0$). $n = 38$ cells from 3 separate experiments.

Approximately 20, 34, and 27% of cells exhibited angularities with magnitude at most 45° and therefore horizontal motion on RG2, DG1 and DG2, respectively (Figure 9A–C). On both DGs, the trajectory of fibroblasts was primarily radial and not horizontal. It is of interest to note that only on DG2 do cells ($\sim 18\%$) move in a perpendicular manner along the “y” axis. The corresponding value is approximately 3% on RG2 and DG1. The perpendicular motion can be attributed to fibroblasts moving up and down at the low-modulus/high-collagen edge of the interfacial region.

Actin Cytoskeleton and Vinculin Localization. The actin cytoskeleton on the low-modulus/high-protein side of the interface did exhibit differences for cells migrating either on DG1 or DG2 (Figure 10A, C). For cells on DG1, the actin filaments were well-defined and were present through the entire cross-section of cells. In contrast, on DG2, the actin filaments were well-defined primarily on the peripheral regions of the cell. Vinculin-enriched focal adhesions were found in the frontal regions of cells on both gradients (Figure 10B, D). Vinculin is a focal adhesion protein that plays a critical role in migration through its presence in nascent focal adhesions.^{7,55} For example, cells lacking vinculin have been reported to be highly motile on 2D substrates.^{56–58} Cells located on the high collagen/low modulus regions of the interface exhibited a greater number of vinculin-enriched focal adhesions than those on the low collagen/high modulus regions. This suggests greater cellular adhesion to the high collagen/low modulus regions, due to a higher collagen concentration. Because of the differences we observed in the expression of vinculin in cells on the ends of the interface, we sought to examine if there were additional differences in their migratory behavior. By dividing

the interfacial region into three distinct regions, each with a width of, $50 \mu\text{m}$ we were able to monitor cellular displacement based upon the initial coordinate of each cells. The average displacement for cells in each region was calculated and analyzed for statistical significance. For fibroblasts on DG1, the average displacement of cells (on Regions 1, 2, and 3) did not result in statistically different average displacements ($p > 0.05$, Table S2). However, on DG2, fibroblasts exhibited a significant decrease in average displacement from the high modulus/low protein region to the low modulus/high protein region ($p = 0.0459$, Table S2). This decrease in cell motility corresponds to the increased presence of vinculin focal adhesions in cells on the low modulus/high protein regions, as shown in previous studies.

DISCUSSION

Durotaxis is a well-studied migratory characteristic that has been reported on a wide range of cells and substrates.²³ We have previously reported cells moving away from stiff (high-modulus) regions in favor of softer domains of a hydrogel.⁴⁶ In this report, there was a sharp increase in YM values of either side of an interface and the soft regions were modified with high concentrations of collagen-coated microspheres. Previously, fibroblast migration in microfluidics devices was investigated where the cells experienced both protein and shear stress gradients.⁵⁹ To the best of our knowledge, there are no migration studies conducted *in vitro* on opposing rigidity-immobilized protein gradients.

We have designed novel opposing rigidity and surface-bound protein gradients using custom designed photomasks and UV-

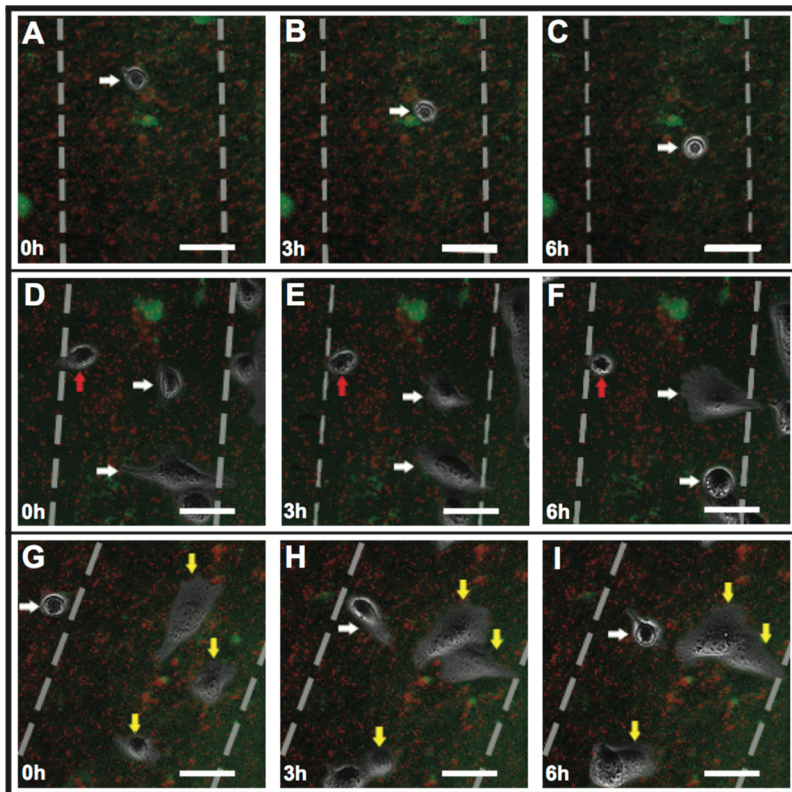


Figure 7. Merged phase-contrast and fluorescence time-lapse images of fibroblasts migrating on (A–C) DG1, (D–F) DG2, and (G–I) DG2. Images D–F depict cells within the gradient exhibiting directed motion toward the low-modulus/high collagen regions. Images G–I depict one cell that is initially located outside the gradient (on the high-modulus region) moving toward the low-modulus/high regions. Scale bars = 50 μm .

Table 4. Direction of Fibroblast Migration on Opposing Rigidity/Protein Gradients

Direction of motion	DG1 n = 29	DG2 n = 33
high-modulus/low collagen to low-modulus/high collagen	15	20
low-modulus/high collagen to high-modulus/low collagen	11	9
exhibiting random walk motion near the low-modulus/high collagen edge of the interfacial region	3	4
p-value of binomial test	0.004	3×10^{-5}

mediated polymerization and conjugation. This approach is inherently versatile and can be extended to design gradients spanning a wide range of elastic moduli. In our work, we have conjugated collagen but virtually any protein can be immobilized using this approach. We assembled two different rigidity gradients to study durotaxis. The broad range of elastic moduli exhibited by the rigidity gradients are of physiological relevance to tissues such as skin, breast, and collagenous bone.^{60–62} Although every attempt was made to obtain mechanical gradients of equal widths, RG2 was significantly wider than RG1. We believe that differential transmission of incident UV between Masks 1 (70%/40%) and 2 (80%/30%) and light scattering led to a wider gradient. Although high-resolution masks (2 $\mu\text{m}/\text{pixel}$) were used to control the degree of incident UV light, it is likely that even greater resolution is required to prevent light scattering. Future studies will focus on using masks with even greater resolution or to choose combinations of gray scale values that exhibit the same differential.

Upon superimposing an immobilized collagen gradient in the opposite direction, a reversal of durotaxis was observed. This reversal occurred by increasing the concentration of immobilized collagen by a factor of 4 or seven from the stiff side to the soft side of the rigidity gradient. It is evident that when fibroblasts preferred low-modulus regions that exhibited a 7-fold increase in collagen. We also investigated the height of the hydrogel at the edges of the interface to determine if topography played a role. The height of the hydrogel on the low- and high-modulus edges did not vary significantly as a function of cross-linking. The heights of the high and low modulus edges were within 12% of the thickness at the middle. The increase in cell areas and decrease in displacement on DG2 can be correlated to the increased adhesivity of the substrate resulting from higher surface-bound collagen at the middle of the interface and on the low-modulus regions. Because the widths of the DGs were approximately 150 μm , the angularity in cell motion was calculated to determine whether cells would choose the quickest route to reach their preferred destination. Based on our data, fibroblasts on RG2 and DG1 primarily exhibited radial motion. Only on DG2 did cells exhibit close to perpendicular motion. These cells were very close to the boundary of the interface on the ~46 kPa/high collagen side. There was a moderate difference between cells exhibiting horizontal trajectories on DG1 and DG2. Although the precise reasons for the observed differences in angularity of cell motion between the two dual gradients are not fully understood, we hypothesize that the higher collagen concentration on DG2 could have played a role. A significant finding was the extent of infiltration was different on the dual gradients. Fibroblasts migrated further into the low modulus/high protein region only

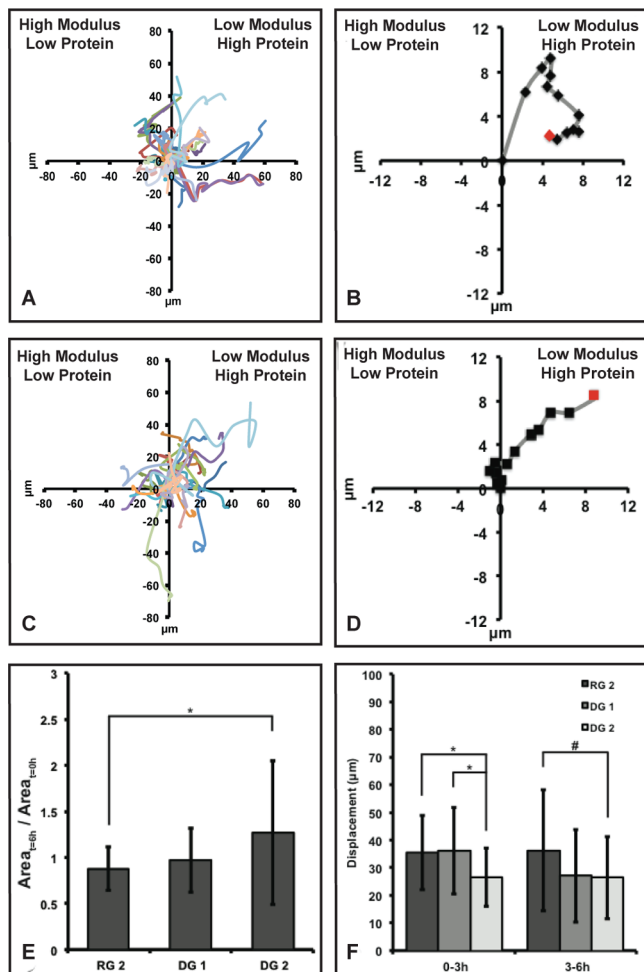


Figure 8. Individual tracks of all cells analyzed on the dual gradients (A) DG1 and (C) DG2. The average trajectory of all cells analyzed on dual gradients (B) DG1 and (D) DG2. The diagrams show positions at each time-point relative to the cell's initial position ($t = 0$). (E) Average area fold change exhibited by fibroblasts over 6 h on RG2, DG1, and DG2. (F) Average displacements exhibited by fibroblasts over 3 h increments on RG2, DG1, and DG2. An asterisk (*) or pound (#) sign indicates a statistically significant difference ($p < 0.05$). $n = 34$ cells from 3 separate experiments (RG2), $n = 29$ cells from 5 separate experiments (DG1), and $n = 33$ cells from 4 separate experiments (DG2).

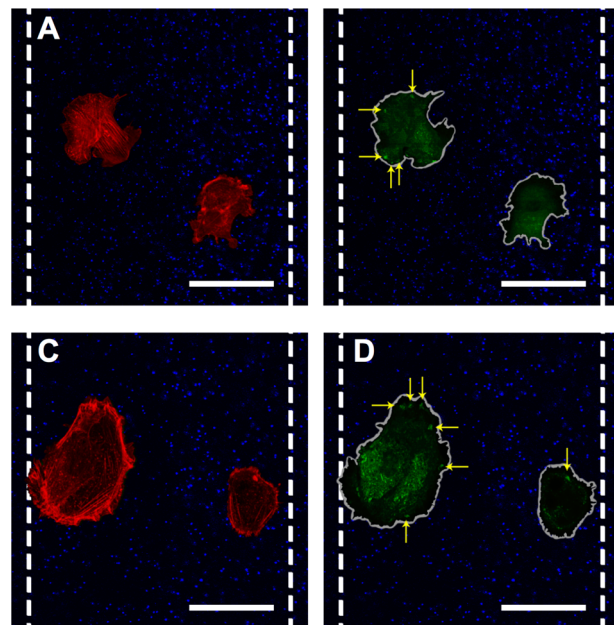


Figure 10. Fluorescent images of actin cytoskeleton and vinculin focal adhesions for fibroblasts on (A, B) DG1 and (C, D) DG2. Actin is depicted in red, vinculin in green, and the embedded polystyrene beads in blue. The vertical dotted lines correspond to the boundaries of the interfacial region. In these images, the high protein, soft side is on the left and the low protein, stiff side on the right. (B, D) Yellow arrows point to focal adhesions. Scale bars = 50 μ m.

when the collagen concentration was increased by 7-fold. These findings are of significance to understand wound healing processes and cancer metastasis.

In this study, we have demonstrated that on hydrogels where the substrate elasticity gradually changes in a direction opposite to the rigidity gradient. In the future, substrates that exhibit lower values of elastic modulus (<15 kPa) with high concentrations of chemokines, cytokines and other ECM proteins may provide insights on how cells migrate into diseased tissues. The current work can be extended into understanding cell migration during wound healing. For example, during the early stages of injury, a mechanical gradient is formed from the interior of the wound (low modulus) to the exterior (high modulus). In addition to the

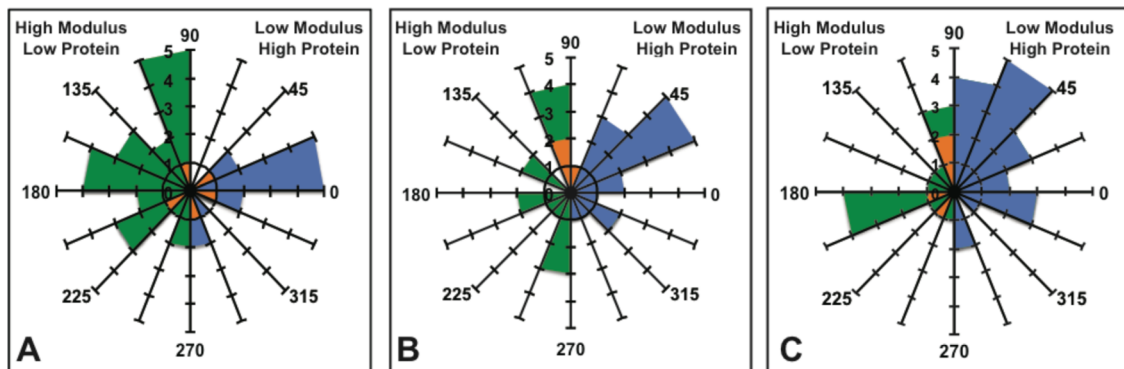


Figure 9. Angularity histograms for (A) RG2, (B) DG1, and (C) DG2, where the angle is determined by the inverse tangent of $(y_f - y_o)/(x_f - x_o)$ where (x_o, y_o) and (x_f, y_f) correspond to the initial (0h) and final (6h) coordinates of cell, respectively. An asterisk (*) or pound (#) indicate a statistically significant difference ($p < 0.05$). $n = 34$ cells from 3 separate experiments (RG2), $n = 29$ cells from 5 separate experiments (DG1), and $n = 33$ cells from 4 separate experiments (DG2).

mechanical gradient, the concentration of signaling molecules is higher in the center of the wound and lower in the periphery.⁶³

CONCLUSIONS

We have designed opposing rigidity–protein gradients. The range of elastic moduli exhibited by these gradients spans a broad range and can therefore be used to investigate cellular migration in different tissues. Since cell locomotion is a dynamic process governed by several stimuli acting simultaneously, we envision that seeking to address how cells move in the presence of dual conflicting stimuli will be of physiological relevance to probe healthy and diseased tissues. The insights obtained on such complex interfaces can aid in the design of future biomaterials and implants that emulate interfacial regions found *in vivo*. Substrates that incorporate multiple stimuli with gradients in different directions could serve as physiologically relevant models to monitor how a cell chooses to move and how one signal may exert a more dominant role than another. In the future, the insights obtained from this work can be extended to investigating migratory behavior during regeneration, cancer metastasis, and wound healing.

ASSOCIATED CONTENT

Supporting Information

The Supporting Information is available free of charge on the ACS Publications website at DOI: [10.1021/acsbiomaterials.Sb00229](https://doi.org/10.1021/acsbiomaterials.Sb00229).

Time-lapse of cells migrating on rigidity gradients, Video S1 ([MOV](#))

Time-lapse of cells migrating on rigidity gradients, Video S2 ([MOV](#))

Time-lapse of cells migrating on opposing rigidity/protein gradients, Video S3 ([MOV](#))

Time-lapse of cells migrating on opposing rigidity/protein gradients, Video S4 ([AVI](#))

Figure S1 and Tables S1 and S2 ([PDF](#))

AUTHOR INFORMATION

Corresponding Author

*E-mail: padmar@vt.edu. Tel: 540-231-4851. Fax: 540-231-5022.

Author Contributions

[†]G.J. and A.J.F. are joint first authors.

Notes

The authors declare no competing financial interest.

ACKNOWLEDGMENTS

We gratefully acknowledge financial support from the National Science Foundation (NSF CAREER DMR-0955873) and the Institute for Critical Technology and Applied Sciences at Virginia Tech.

REFERENCES

- (1) Keller, R. Cell migration during gastrulation. *Curr. Opin. Cell Biol.* **2005**, *17* (5), 533–541.
- (2) Locascio, A.; Nieto, M. A. Cell movements during vertebrate development: integrated tissue behaviour versus individual cell migration. *Curr. Opin. Genet. Dev.* **2001**, *11* (4), 464–469.
- (3) Rorth, P. Collective cell migration. *Annu. Rev. Cell Dev. Biol.* **2009**, *25*, 407–429.
- (4) Yamada, K. M. Fibronectin peptides in cell migration and wound repair. *J. Clin. Invest.* **2000**, *105* (11), 1507–9.
- (5) Luster, A. D.; Alon, R.; von Andrian, U. H. Immune cell migration in inflammation: present and future therapeutic targets. *Nat. Immunol.* **2005**, *6* (12), 1182–1190.
- (6) Franz, C. M.; Jones, G. E.; Ridley, A. J. Cell Migration in Development and Disease. *Dev. Cell* **2002**, *2* (2), 153–158.
- (7) Ridley, A. J.; Schwartz, M. A.; Burridge, K.; Firtel, R. A.; Ginsberg, M. H.; Borisy, G.; Parsons, J. T.; Horwitz, A. R. Cell Migration: Integrating Signals from Front to Back. *Science* **2003**, *302* (5651), 1704–1709.
- (8) Chambers, A. F.; Groom, A. C.; MacDonald, I. C. Metastasis: Dissemination and growth of cancer cells in metastatic sites. *Nat. Rev. Cancer* **2002**, *2* (8), 563–572.
- (9) Kolaczkowska, E.; Kubes, P. Neutrophil recruitment and function in health and inflammation. *Nat. Rev. Immunol.* **2013**, *13* (3), 159–75.
- (10) Lamalice, L.; Le Boeuf, F.; Huot, J. Endothelial Cell Migration During Angiogenesis. *Circ. Res.* **2007**, *100* (6), 782–794.
- (11) Marin, O.; Rubenstein, J. L. R. Cell migration in the forebrain. *Annu. Rev. Neurosci.* **2003**, *26* (1), 441–483.
- (12) Yamaguchi, H.; Wyckoff, J.; Condeelis, J. Cell migration in tumors. *Curr. Opin. Cell Biol.* **2005**, *17* (5), 559–564.
- (13) Singer, A. J.; Clark, R. A. F. Cutaneous Wound Healing. *N. Engl. J. Med.* **1999**, *341* (10), 738–746.
- (14) Nguyen, D. X.; Bos, P. D.; Massague, J. Metastasis: from dissemination to organ-specific colonization. *Nat. Rev. Cancer* **2009**, *9* (4), 274–284.
- (15) Petrie, R. J.; Doyle, A. D.; Yamada, K. M. Random versus directionally persistent cell migration. *Nat. Rev. Mol. Cell Biol.* **2009**, *10* (8), 538–549.
- (16) Lo, C.-M.; Wang, H.-B.; Dembo, M.; Wang, Y.-l. Cell Movement Is Guided by the Rigidity of the Substrate. *Biophys. J.* **2000**, *79* (1), 144–152.
- (17) Pelham, R. J.; Wang, Y.-l. Cell locomotion and focal adhesions are regulated by substrate flexibility. *Proc. Natl. Acad. Sci. U. S. A.* **1997**, *94* (25), 13661–13665.
- (18) Brown, M. J.; Loew, L. M. Electric field-directed fibroblast locomotion involves cell surface molecular reorganization and is calcium independent. *J. Cell Biol.* **1994**, *127* (1), 117–128.
- (19) Saranak, J.; Foster, K. W. Rhodopsin guides fungal phototaxis. *Nature* **1997**, *387* (6632), 465–466.
- (20) Han, L.; Mao, Z.; Wu, J.; Guo, Y.; Ren, T.; Gao, C. Directional cell migration through cell-cell interaction on polyelectrolyte multilayers with swelling gradients. *Biomaterials* **2013**, *34* (4), 975–84.
- (21) Vaday, G. G.; Franitz, S.; Schor, H.; Hecht, I.; Brill, A.; Cahalon, L.; Hershkoviz, R.; Lider, O. Combinatorial signals by inflammatory cytokines and chemokines mediate leukocyte interactions with extracellular matrix. *Journal of leukocyte biology* **2001**, *69* (6), 885–92.
- (22) Savino, W.; Mendes-da-Cruz, D. A.; Silva, J. S.; Dardenne, M.; Cotta-de-Almeida, V. Intrathymic T-cell migration: a combinatorial interplay of extracellular matrix and chemokines? *Trends Immunol.* **2002**, *23* (6), 305–13.
- (23) Sant, S.; Hancock, M. J.; Donnelly, J. P.; Iyer, D.; Khademhosseini, A. Biomimetic Gradient Hydrogels for Tissue Engineering. *Can. J. Chem. Eng.* **2010**, *88* (6), 899–911.
- (24) Lee, E. J.; Kasper, F. K.; Mikos, A. G. Biomaterials for tissue engineering. *Ann. Biomed. Eng.* **2014**, *42* (2), 323–37.
- (25) Yang, P. J.; Temenoff, J. S. Engineering Orthopedic Tissue Interfaces. *Tissue Eng., Part B* **2009**, *15* (2), 127–141.
- (26) Ladd, M. R.; Lee, S. J.; Stitzel, J. D.; Atala, A.; Yoo, J. J. Co-electrospun dual scaffolding system with potential for muscle-tendon junction tissue engineering. *Biomaterials* **2011**, *32* (6), 1549–59.
- (27) Laurencin, C. T.; Freeman, J. W. Ligament tissue engineering: An evolutionary materials science approach. *Biomaterials* **2005**, *26* (36), 7530–7536.
- (28) Wu, J.; Mao, Z.; Tan, H.; Han, L.; Ren, T.; Gao, C. Gradient biomaterials and their influences on cell migration. *Interface Focus* **2012**, *2* (3), 337–55.

- (29) Guelcher, S. A.; Sterling, J. A. Contribution of bone tissue modulus to breast cancer metastasis to bone. *Cancer Microenviron.* **2011**, *4* (3), 247–59.
- (30) Suva, L. J.; Griffin, R. J.; Makhoul, I. Mechanisms of bone metastases of breast cancer. *Endocr.-Relat. Cancer* **2009**, *16* (3), 703–713.
- (31) Thiery, J. P.; Duband, J. L.; Tucker, G. C. Cell Migration in the Vertebrate Embryo: Role of Cell Adhesion and Tissue Environment in Pattern Formation. *Annu. Rev. Cell Biol.* **1985**, *1* (1), 91–113.
- (32) Jacinto, A.; Martinez-Arias, A.; Martin, P. Mechanisms of epithelial fusion and repair. *Nat. Cell Biol.* **2001**, *3* (5), E117–E123.
- (33) Smith, J. T.; Tomfohr, J. K.; Wells, M. C.; Beebe, T. P.; Kepler, T. B.; Reichert, W. M. Measurement of Cell Migration on Surface-Bound Fibronectin Gradients. *Langmuir* **2004**, *20* (19), 8279–8286.
- (34) Zigmond, S. H. Ability of polymorphonuclear leukocytes to orient in gradients of chemotactic factors. *J. Cell Biol.* **1977**, *75* (2), 606–616.
- (35) Zaari, N.; Rajagopalan, P.; Kim, S. K.; Engler, A. J.; Wong, J. Y. Photopolymerization in Microfluidic Gradient Generators: Microscale Control of Substrate Compliance to Manipulate Cell Response. *Adv. Mater.* **2004**, *16* (23–24), 2133–2137.
- (36) Li Jeon, N.; Baskaran, H.; Dertinger, S. K. W.; Whitesides, G. M.; Van De Water, L.; Toner, M. Neutrophil chemotaxis in linear and complex gradients of interleukin-8 formed in a microfabricated device. *Nat. Biotechnol.* **2002**, *20* (8), 826–830.
- (37) Chen, G.; Ito, Y. Gradient micropattern immobilization of EGF to investigate the effect of artificial juxtacline stimulation. *Biomaterials* **2001**, *22* (18), 2453–2457.
- (38) DiMilla, P.; Stone, J.; Quinn, J.; Albelda, S.; Lauffenburger, D. Maximal migration of human smooth muscle cells on fibronectin and type IV collagen occurs at an intermediate attachment strength. *J. Cell Biol.* **1993**, *122* (3), 729–737.
- (39) Seppä, H.; Grotendorst, G.; Seppä, S.; Schiffmann, E.; Martin, G. R. Platelet-derived growth factor in chemotactic for fibroblasts. *J. Cell Biol.* **1982**, *92* (2), 584–588.
- (40) Stefonek, T. J.; Masters, K. S. Immobilized gradients of epidermal growth factor promote accelerated and directed keratinocyte migration. *Wound Repair and Regeneration* **2007**, *15* (6), 847–855.
- (41) Lin, F.; Nguyen, C. M.-C.; Wang, S.-J.; Saadi, W.; Gross, S. P.; Jeon, N. L. Effective neutrophil chemotaxis is strongly influenced by mean IL-8 concentration. *Biochem. Biophys. Res. Commun.* **2004**, *319* (2), 576–581.
- (42) Barkefors, I.; Le Jan, S.; Jakobsson, L.; Hejll, E.; Carlson, G.; Johansson, H.; Jarvius, J.; Park, J. W.; Li Jeon, N.; Kreuger, J. Endothelial cell migration in stable gradients of vascular endothelial growth factor A and fibroblast growth factor 2: effects on chemotaxis and chemokinesis. *J. Biol. Chem.* **2008**, *283* (20), 13905–13912.
- (43) Hadjipanayi, E.; Mudera, V.; Brown, R. A. Guiding cell migration in 3D: a collagen matrix with graded directional stiffness. *Cell Motil. Cytoskeleton* **2009**, *66* (3), 121–8.
- (44) Sundararaghavan, H. G.; Burdick, J. A. Gradients with depth in electrospun fibrous scaffolds for directed cell behavior. *Biomacromolecules* **2011**, *12* (6), 2344–50.
- (45) Kim, I. L.; Khetan, S.; Baker, B. M.; Chen, C. S.; Burdick, J. A. Fibrous hyaluronic acid hydrogels that direct MSC chondrogenesis through mechanical and adhesive cues. *Biomaterials* **2013**, *34* (22), 5571–5580.
- (46) Hale, N. A.; Yang, Y.; Rajagopalan, P. Cell Migration at the Interface of a Dual Chemical-Mechanical Gradient. *ACS Appl. Mater. Interfaces* **2010**, *2* (8), 2317–2324.
- (47) Rajagopalan, P.; Marganski, W. A.; Brown, X. Q.; Wong, J. Y. Direct comparison of the spread area, contractility, and migration of balb/c 3T3 fibroblasts adhered to fibronectin- and RGD-modified substrata. *Biophys. J.* **2004**, *87* (4), 2818–27.
- (48) Wong, J. Y.; Velasco, A.; Rajagopalan, P.; Pham, Q. Directed Movement of Vascular Smooth Muscle Cells on Gradient-Compliant Hydrogels†. *Langmuir* **2003**, *19* (5), 1908–1913.
- (49) Tse, J. R.; Engler, A. J., Preparation of Hydrogel Substrates with Tunable Mechanical Properties. In *Current Protocols in Cell Biology*; John Wiley & Sons: New York, 2001.
- (50) Geissler, E.; Hecht, A. M. The Poisson Ratio in Polymer Gels. *Macromolecules* **1980**, *13* (5), 1276–1280.
- (51) Engler, A.; Bacakova, L.; Newman, C.; Hategan, A.; Griffin, M.; Discher, D. Substrate Compliance versus Ligand Density in Cell on Gel Responses. *Biophys. J.* **2004**, *86* (1), 617–628.
- (52) Gaudet, C.; Marganski, W. A.; Kim, S.; Brown, C. T.; Gunderia, V.; Dembo, M.; Wong, J. Y. Influence of Type I Collagen Surface Density on Fibroblast Spreading, Motility, and Contractility. *Biophys. J.* **2003**, *85* (5), 3329–3335.
- (53) Walsh, B. J.; Thornton, S. C.; Penny, R.; Breit, S. N. Microplate reader-based quantitation of collagens. *Anal. Biochem.* **1992**, *203* (2), 187–90.
- (54) Salmon, H.; Rivas-Caicedo, A.; Aspert-Boursin, F.; Lebugle, C.; Bourdoncle, P.; Donnadieu, E. Ex vivo imaging of T cells in murine lymph node slices with widefield and confocal microscopes. *J. Visualized Exp.* **2011**, *53*, e3054.
- (55) Zaidel-Bar, R.; Ballestrem, C.; Kam, Z.; Geiger, B. Early molecular events in the assembly of matrix adhesions at the leading edge of migrating cells. *J. Cell Sci.* **2003**, *116* (Pt 22), 4605–13.
- (56) Subauste, M. C.; Pertz, O.; Adamson, E. D.; Turner, C. E.; Junger, S.; Hahn, K. M. Vinculin modulation of paxillin-FAK interactions regulates ERK to control survival and motility. *J. Cell Biol.* **2004**, *165* (3), 371–381.
- (57) Saunders, R. M.; Holt, M. R.; Jennings, L.; Sutton, D. H.; Barsukov, I. L.; Bobkov, A.; Liddington, R. C.; Adamson, E. A.; Dunn, G. A.; Critchley, D. R. Role of vinculin in regulating focal adhesion turnover. *Eur. J. Cell Biol.* **2006**, *85* (6), 487–500.
- (58) Mierke, C. T.; Kollmannsberger, P.; Zitterbart, D. P.; Diez, G.; Koch, T. M.; Marg, S.; Ziegler, W. H.; Goldmann, W. H.; Fabry, B. Vinculin facilitates cell invasion into three-dimensional collagen matrices. *J. Biol. Chem.* **2010**, *285* (17), 13121–30.
- (59) Park, J. Y.; Yoo, S. J.; Hwang, C. M.; Lee, S. H. Simultaneous generation of chemical concentration and mechanical shear stress gradients using microfluidic osmotic flow comparable to interstitial flow. *Lab Chip* **2009**, *9* (15), 2194–202.
- (60) Kirkpatrick, S. J.; Wang, R. K.; Duncan, D. D.; Kulesz-Martin, M.; Lee, K. Imaging the mechanical stiffness of skin lesions by in vivo acousto-optical elastography. *Opt. Express* **2006**, *14* (21), 9770–9.
- (61) Rzymski, P.; Skorzewska, A.; Skibinska-Zielinska, M.; Opala, T. Factors influencing breast elasticity measured by the ultrasound Shear Wave elastography - preliminary results. *Arch. Med. Sci.* **2011**, *7* (1), 127–133.
- (62) Engler, A. J.; Sen, S.; Sweeney, H. L.; Discher, D. E. Matrix elasticity directs stem cell lineage specification. *Cell* **2006**, *126* (4), 677–89.
- (63) Shaw, T. J.; Martin, P. Wound repair at a glance. *J. Cell Sci.* **2009**, *122* (18), 3209–3213.